

Current Flow in Vibrissa Motor Cortex Can Phase-Lock With Exploratory Rhythmic Whisking in Rat

Kurt F. Ahrens^{1,3} and David Kleinfeld^{1,2}

¹Department of Physics and ²Neurosciences Graduate Program, University of California at San Diego, La Jolla, California 92093; and

³Center for Molecular and Behavioral Neuroscience, Rutgers University, Newark, New Jersey 07102

Submitted 8 January 2004; accepted in final form 4 April 2004

Ahrens, Kurt F. and David Kleinfeld. Current flow in vibrissa motor cortex can phase-lock with exploratory rhythmic whisking in rat. *J Neurophysiol* 92: 1700–1707, 2004. First published April 7, 2004; 10.1152/jn.00020.2004. Rats explore their environment with rhythmic sweeps of their mystacial vibrissae in the range of 5–15 Hz. We tested if vibrissa primary motor (M1) cortex produces electrical activity that locks to this behavioral output. Rats were trained to whisk in air in search of a food reward. The EMG of the mystacial pad served as a surrogate of vibrissa position, while chronically implanted, 16-channel Si-based probes provided a record of field potentials throughout the depth of vibrissa M1 cortex as well as vibrissa primary somatosensory (S1) cortex. The measured potentials were used to estimate the current source density along the radial axis. We observed that current flow throughout the depth of M1 cortex is coherent with the mystacial EMG, i.e., the two signals co-vary with a defined phase relation. This coherence persists after transection of the infraorbital branch (IoN) of the trigeminal nerve, which provides the sole sensory input from the vibrissae. Furthermore, current flow in vibrissa S1 cortex that is coherent with the mystacial EMG also persists after transection of the IoN, consistent with anatomical pathways between M1 and S1. In combination with a previous observation that rhythmic, intracortical microstimulation of vibrissa M1 cortex can drive normal whisking motion, the present data support the hypothesis that, in principle, M1 cortex can initiate motion of the vibrissae on a cycle-by-cycle basis.

INTRODUCTION

Rats explore their local environment with active whisking of their mystacial vibrissae as a means to localize objects and discriminate among them based on shape and texture (Brecht et al. 1997; Carvell and Simons 1990; Hutson and Masterton 1986; Mehta and Kleinfeld 2004). Rhythmic sweeps, in which the vibrissae are successively protracted and retracted at a rate that ranges from 5 to 15 Hz, occur in sustained bouts of whisking that extend ≥ 1 s (Berg and Kleinfeld 2003a; Welker 1964). Previous studies have shown that spike activity in vibrissa primary motor (M1) cortex increases during bouts of whisking (Carvell et al. 1996). An open issue, however, is whether electrical activity in motor cortex varies in phase with whisking. Substantial phase-locking between the two signals would establish that M1 cortex can, as matter of principle, exert cycle-by-cycle control over whisking. Such control may come into play with tasks that require a high level of sensory feedback, in analogy with predictive cortical signals in the control of fine hand movements in monkeys (Moran and Schwartz 1999).

Here we address the nature of signaling in vibrissa M1 cortex in animals trained to whisk in air (Berg and Kleinfeld 2003a; Fee et al. 1997; O'Connor et al. 2002). We measure current flow in cortex through the use of multisite electrodes (Ahrens and Freeman 2001; Ahrens et al. 2002; Kandel and Buzsaki 1997), and we use the EMG of the mystacial pad to infer movement of the vibrissa (Berg and Kleinfeld 2003a; Carvell et al. 1991). We ask the following questions. 1) Is there an electrical signal in vibrissa M1 cortex that is phase-locked with the rhythmic movement of the vibrissa? 2) If so, does this signal, and the known phase-locked current flow in vibrissa S1 cortex (Jones and Barth 1999; O'Connor et al. 2002), persist after transection of the infraorbital branch (IoN) of the trigeminal nerve to block all sensory input?

This study is motivated by three bodies of work. First, there are extensive intercortical projections from S1 to M1 cortices (Hoffer et al. 2003; Izraeli and Porter 1995; Keller et al. 1996; Kim and Ebner 1999). These maintain the topography of the vibrissa organization, with the majority of axons originating in layer 5 of S1 cortex and terminating in superficial layers of M1 cortex (Izraeli and Porter 1995). Furthermore, a subcortical pathway that involves posterior medial thalamus receives feedback projections from both M1 and S1 cortices and provides common input to the granular layers in these two cortical areas (Deschenes et al. 1998). Thus there is an anatomical substrate for at least an afferent copy of vibrissa motion to reach circuits in M1 cortex. Second, unit activity in M1 cortex displays a sensory response that follows periodic stimulation of the vibrissae (Kleinfeld et al. 2002). The amplitude of this response is constant throughout the frequency range of normal whisking (Kleinfeld et al. 2002). Thus circuits in motor cortex not only receive sensory input but have the temporal speed to fire in phase with whisking. Last, intracellular stimulation of neurons in M1 cortex leads to rapid motion of individual vibrissae (Brecht et al. 2004). In addition, extracellular microstimulation of M1 cortex in awake and aroused animals, as opposed to sessile animals and anesthetized animals, can drive the muscular sequence of protraction and retraction of the vibrissae that occurs during normal whisking (Berg and Kleinfeld 2003b). Thus in principle, circuits in motor cortex can drive normal whisking. Taken together, these three lines of evidence support the hypothesis that M1 cortex can integrate vibrissa sensory feedback and motor drive signals on the time-scale of the whisking cycle. This implies that circuits in

Address for reprint requests and other correspondence: D. Kleinfeld, Dept. of Physics 0374, Univ. of California, 9500 Gilman Dr., La Jolla, CA 92093 (E-mail: dk@physics.ucsd.edu).

The costs of publication of this article were defrayed in part by the payment of page charges. The article must therefore be hereby marked "advertisement" in accordance with 18 U.S.C. Section 1734 solely to indicate this fact.

vibrissa M1 cortex should exhibit rhythmic activity that is phase-locked to whisking.

METHODS

We report data from five Long-Evans female rats, 200–350 g in mass. Additional animals were prepared to optimize our training paradigm and recording parameters. The care and experimental manipulation of our animals were in strict accord with guidelines from the National Institutes of Health (1985) and have been reviewed and approved by the Institutional Animal Care and Use Committee at the University of California, San Diego. The sequence of procedures, described in detail below, is summarized as follows: Training → Surgery → Retraining → Recording → IoN Lesion → Recording → Histology.

Training

Rats were calmed by handling and free exploration of a loop-shaped platform with a perch for 0.5–1 h/day for the first 3–5 days. Following acclimatization, the animals were placed on a diet of liquid food [50% (wt/vol); LD-100, PMI Feeds, Newco Distributors, Rancho Cucamonga, CA], the task reward, ad libitum. As soon as they became accustomed to both the platform and this food, the rats were trained to crane at the perch and search for and feed at a robotic arm that dispensed the liquid food contingent on correct navigation of the loop (Berg and Kleinfeld 2003a; Fee et al. 1997). Supplemental food was made available to maintain good health as required.

Surgery was performed to implant electrodes and to suture the eyelids of the animals. The animals were subsequently retrained to search for and feed at the robotic arm. A variable delay period between the onset of the search and the delivery of the arm served to elicit extended periods of exploratory whisking. Frequently the rats would search in the same locale after the food tube had been removed, which resulted in additional periods of whisking.

Surgical procedures

Animals were anesthetized with 2% halothane in humidified O₂ and secured in a stereotaxic holder in the flat-skull position (Paxinos and Watson 1986). Temperature was maintained at 37°C throughout surgery and recovery. The preparation and implantation of the 16-channel Si-based multielectrode probe (3 mm100 or 10 mm100; Center for Neural Communication Technology, University of Michigan, Ann Arbor, MI) has been described (Ahrens et al. 2002; Prechtl et al. 2000). In brief, a single midline incision was made, tissue was reflected from the skull dorsum and the dorsal region of the temporal bones, and rectangular windows that extended from 1 to 3 mm anterior to Bregma and from 1 to 2 mm lateral to the midline for M1 cortex, and from 2 to 4 mm posterior to Bregma and from 4 to 6 mm lateral to the midline for S1 cortex, were opened. A fine incision to the dura mater in each window was made with the tip of a 30-gauge hypodermic needle. A Si-probe was placed in the center of each incision, lowered into the brain, secured, and cabled, as described (Ahrens et al. 2002). Last, 50- μ m-diam Teflon-insulated tungsten wires were threaded into the mystacial pad and set to lie about halfway through the vibrissa field, as described (Fee et al. 1997), to record the EMG.

Surgical eyelid closure was performed to prevent the use of visual cues during the behavioral task. After recovery from the electrode implantation surgery and reacclimation to the recording apparatus, the animals were anesthetized with ketamine and xylazine. The skin surrounding each eye was shaved and treated with povidone iodine. The margins of the eyelids were trimmed with iridectomy scissors, and the margins were lightly compressed in opposition with a clamp of local design and sewn together with 5–0 monofilament suture material. Antibiotic ophthalmic ointment was applied daily until the eyelids were fused, and the sutures were removed after 5–7 days.

Recordings

Potentials throughout the depth of vibrissa S1 and M1 cortex were obtained simultaneously with the Si-based arrays. The signals from each electrode were impedance-buffered, amplified, filtered (0.3-Hz single-pole high-pass and 75-Hz 6-pole Bessel low-pass), and digitized (500 Hz) as described (Ahrens et al. 2002). The voltage signals measured along each array were used to calculate the second spatial derivative of the potential with respect to depth. This signal, referred to as the current-source density (CSD) (Mitzdorf 1987; Nicholson and Freeman 1975), was estimated as $CSD \cong -[V(z + \Delta z, t) - 2V(z, t) + V(z - \Delta z, t)]/\Delta z^2$, where $V(z, t)$ is the measured voltage at a depth z , and $\Delta z = 100 \mu\text{m}$.

The signals from the EMG were impedance-buffered in the same manner as the signals from the Si-array. They were subsequently high-pass filtered at 80 Hz (4-pole linear phase filter constructed with a model UAF42 building block; Burr Brown, Tucson, AZ), full-wave rectified, and low-pass filtered at 100 Hz (4-pole linear phase filter; Frequency Devices, Haverhill, MA) to produce the envelope of vibrissa muscle activity. The rectified EMG signals were likewise digitized.

Multitaper spectral estimation methods (Thomson 1982) were used to compute the spectral power density of CSD and EMG time series, as well as the spectral coherence between these signals, as averages across a frequency band and trials. Confidence intervals for the coherence were estimated using the formula of Jarvis and Mitra (2001), as previously described (Ahrens et al. 2002).

Anesthetized responses

Stimulus-evoked responses were recorded within 2–4 days subsequent to surgery. The animals were anesthetized with intramuscular injections of ketamine (50 mg/kg rat) and xylazine (10 mg/kg rat); atropine was further administered (0.05 mg/kg rat). Anesthesia was supplemented with 30% of initial dose on the occurrence of pedal or corneal reflexes. Subsets of five to six mystacial vibrissae were captured in a fine mesh and stimulated with a piezoelectric drive of local design (Kleinfeld and Delaney 1996). The maximum amplitude of the deflection was typically $\pm 1^\circ$, and the square pulse of stimulus drive was filtered (4-pole Bessel low-pass filter) to achieve a rise time of 5 ms; this prevented mechanical resonances of the piezoelectric drive. Typically, 100 stimuli were presented, with each stimulus delivered at the 1-s time point of a 3-s record.

Lesion of the IoN

Transection of the infraorbital branch of the trigeminal nerve was performed in four of the animals, as described (Berg and Kleinfeld 2003a). The completeness of the lesion was immediately tested by measuring the evoked response in vibrissa S1 cortex and confirmed by direct observation at the time of perfusion.

Histology

At the termination of experiments, the rats were killed by lethal overdose of anesthetic and fixed by transcardial perfusion of buffered saline followed by paraformaldehyde in buffered saline, and their brain was removed and sectioned at 30 μm thickness, mounted, and stained with thionin (Berg and Kleinfeld 2003b).

RESULTS

Response under anesthesia

We consider first the stimulus-evoked electrical activity in animals under anesthesia as a means to verify the correct placement of the silicon probes in vibrissa M1 and S1 cortices.

Local field activity was robustly evoked in the vibrissa regions of M1 cortex as well S1 cortex by brief pulsatile stimuli applied to a grouping of the mystacial vibrissae (Fig. 1, *A* and *B*, *top*). Variation in the local field potential was evident across each 16-channel array of electrodes and indicates a heterogeneous pattern of current flow. A similar variation, albeit of weaker amplitude, was observed in response to single vibrissa

stimulation (data not shown). The approximate positions of the recording sites for these probes were found from the slender tracks in sections prepared from the postmortem tissue (Fig. 1, *A* and *B*, * in *bottom panels*). Minimal, if any, gross damage to cortex was observed.

The CSD calculation provides a measure of the spatial divergence of current flow, or equivalently, sources and sinks

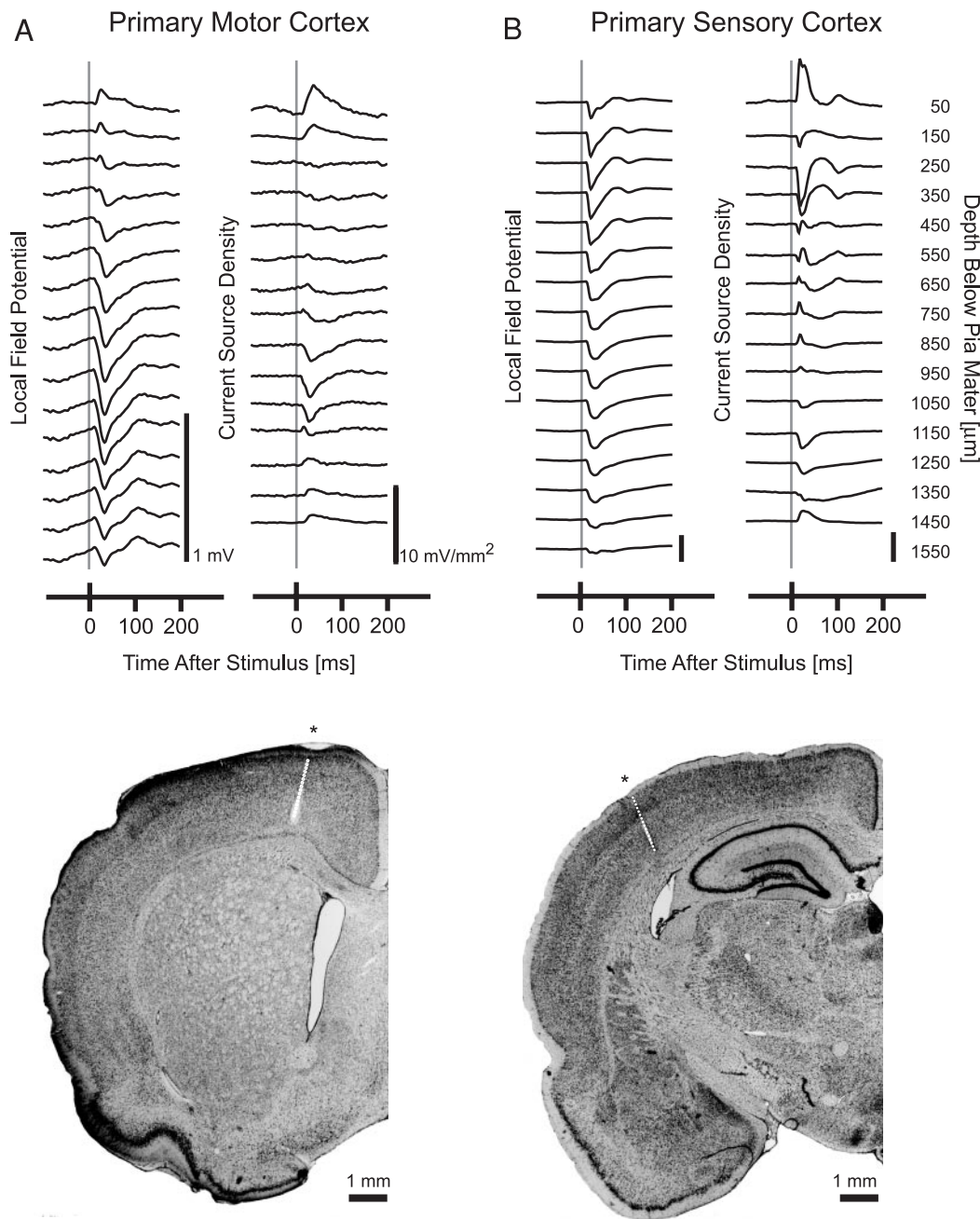


FIG. 1. Evoked current-source density (CSD) signals in the anesthetized rat and histology of the implanted probe positions. *A*: *top*: average local field potentials (LFPs) simultaneously recorded at different depths below the pial surface in vibrissa M1 cortex in response to 100 pulsatile deflections of the vibrissae, with a stimulus period of >3 s. Scale bar is 1 mV. Traces of the *right* are the CSDs derived from the LFP data. Scale bar is 10 mV/mm². Vertical gray lines mark the time of stimulation. *Bottom*: photomicrograph of a 30- μ m thick coronal section of M1 cortex, stained with thionin, that was penetrated by the 16-channel probe. A lesion caused by the probe is seen at a depth of 1,800 μ m below the pia mater. Labeling over the probe track corresponds to approximate positions of individual recording sites, with an interelectrode distance of 100 μ m. *B*: *top*: average LFP simultaneously recorded at different depths below the pial surface in vibrissa S1 cortex, as in *A*. Scale bar is 1 mV. CSD is derived from LFP data. Scale bar is 10 mV/mm². *B*: *bottom*: analogous photomicrograph of S1 cortex. A lesion caused by the probe is seen at a depth of 1,300 μ m below the pia mater. Approximate locations of individual recording sites are marked.

of charge (Nicholson and Freeman 1975). The greatest contribution to the measured current flow in cortex is thought to be excitatory postsynaptic currents, which appear as negative current flows, or sinks (Mitzdorf 1987). The observed CSD is therefore representative of the input to neurons that occurs as part of afferent input as well as local, recurrent activity. The present data compares favorably with the identification of disparate signal generators at different depths within the same neocortical region (Di and Barth 1991; Kandel and Buzsaki 1997). The large negative potentials in the superficial layers are likely to represent thalamic input to the lower part of layers 2/3 and 4, from ventral posterior medial thalamus for S1 cortex and ventral lateral thalamus for M1 cortex, while the negative potentials in deep layers are likely to represent a mixture of inputs from cortico-cortical projections as well as posterior medial thalamic afferents (Deschenes et al. 1998). Last, the amplitude of the CSD as measured in M1 cortex was consistently smaller than that measured at comparable depths in S1 cortex (cf. Fig. 1, A and B). As an average across all animals, the difference in the maximum observed amplitude was approximately a factor of 4 ($n = 4$ animals; Fig. 2A). This difference is consistent with the more pronounced columnar organization in sensory over motor cortices (Keller 1993). As a practical issue, this difference made recording in motor cortex more challenging than recording in sensory cortex.

Responses during exploratory whisking

Rats were trained to find a food tube in free air without the use of vision. Vibrissa contact appeared to be the predominant cue for target localization as opposed to scent, since the animals invariably positioned themselves to lick the end of the tube after the first contact of their vibrissae with the tube. Data from the exploratory periods of free-air whisking prior to the food reward, all 1.5 s or longer in duration, were used for the analyses described here.

Example data illustrate the signals observed during whisking (Fig. 3). A bout of rhythmic vibrissa protraction is seen in the trace of the EMG. The time-frequency plot of the spectrum for this signal shows that the greatest power is at the whisking frequency (Fig. 3, top). Additional power in the second and third harmonics of that frequency is a consequence of the nonsinusoidal waveform of the EMG. The simultaneously recorded CSD from different depths in M1 cortex shows clearly discernible oscillations only at selected depths below the pia (e.g., trace at 1,000 μm ; Fig. 3). These oscillations are seen to be significantly coherent with the EMG (Fig. 3, 2nd spectrogram), i.e., oscillations in current flow in M1 cortex maintain a fixed phase relation with oscillations in the mystacial EMG over the time-course of the whisking epoch. In contrast, and as expected from past work (O'Connor et al. 2002), the CSD signals throughout the depth of S1 cortex exhibit clear oscillations that were significantly coherent with those in the EMG (Fig. 3, 3rd spectrogram). The coherence rose coincident with the onset of whisking (Fig. 3, *). Last, in this example, the oscillatory activity between M1 and S1 cortices was significantly coherent (Fig. 3, bottom).

We continue to focus on the results for individual animals and consider the trial-to-trial variation in the coherence be-

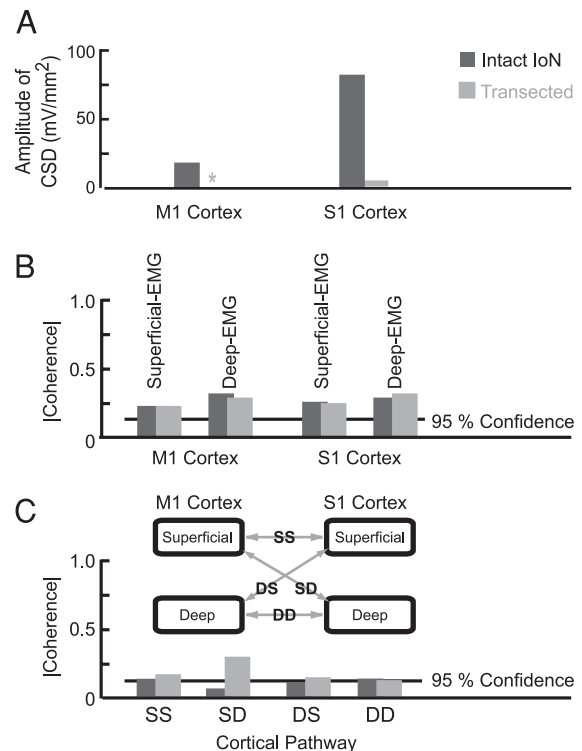


FIG. 2. Summary of CSD measurements and computed spectral coherence across all animals ($n = 5$). A: magnitude of the CSD peak amplitude measured at an average depth below the pia mater of 700 μm in M1 cortex and 500 μm in S1 cortex. Responses were evoked by 100 pulsatile deflections of the vibrissae. Note that evoked motor cortical responses were not evident in any animal following lesion of the infraorbital branch (IoN); the small response observed in S1 cortex resulted from a single animal with only ~90% transection of IoN. B: magnitude of the coherence between cortical CSD and rectified EMG. Analysis is parceled according to superficial vs. deep layers, corresponding to average depths of 700 and 1,200 μm in M1 cortices and 500 and 1,100 μm in S1 cortex, both before ($n = 192$) and after IoN lesion ($n = 136$). C: magnitude of average coherence measured between motor and sensory CSD channels. Significance was reached following IoN lesion between superficial motor and sensory channels and between superficial motor and deep sensory channels. Inset: diagram of functional connections investigated by calculating the coherence between motor and sensory channels. Arrows are bidirectional because for rhythmic signals the coherence indicates a phase relationship between channels, but does not tell whether a given channel is generating the signal or receiving it. For the purpose of cortico-cortical coherence measurements, superficial and deep M1 channels are at average depths of 100 and 1,300 μm , while the superficial and deep S1 channels are at average depths of 200 and 1,200 μm .

tween the motor cortical CSD signals and the EMG (Fig. 4; the magnitude of the coherence is the radial coordinate and the phase is the angular coordinate). The variability of the response, in the sense of a different phase relation between the CSD and the EMG, is greater at the superficial depths of layer 4 to upper layer 5 (Fig. 4A; 500–700 μm below the pia) than at deep layer 5 (Fig. 4B; 1,100–1,200 μm below the pia). Nonetheless, the vector average of the coherence is significant (Fig. 4, A and B; the red bar is the average and the circle is the 95% confidence limit). The frequency dependence of the coherence, averaged over all epochs, has peaks at the whisking frequency and its harmonics with a magnitude that approaches 0.5 at the level of layer 5 (Fig. 4B). In this example, $|C(f)|^2 = 0.25$ of the spectral power in the M1 cortical CSD is locked to variations in the EMG (Mardia et al. 1979). Last, very similar results, in terms of variability and the magnitude of the coher-

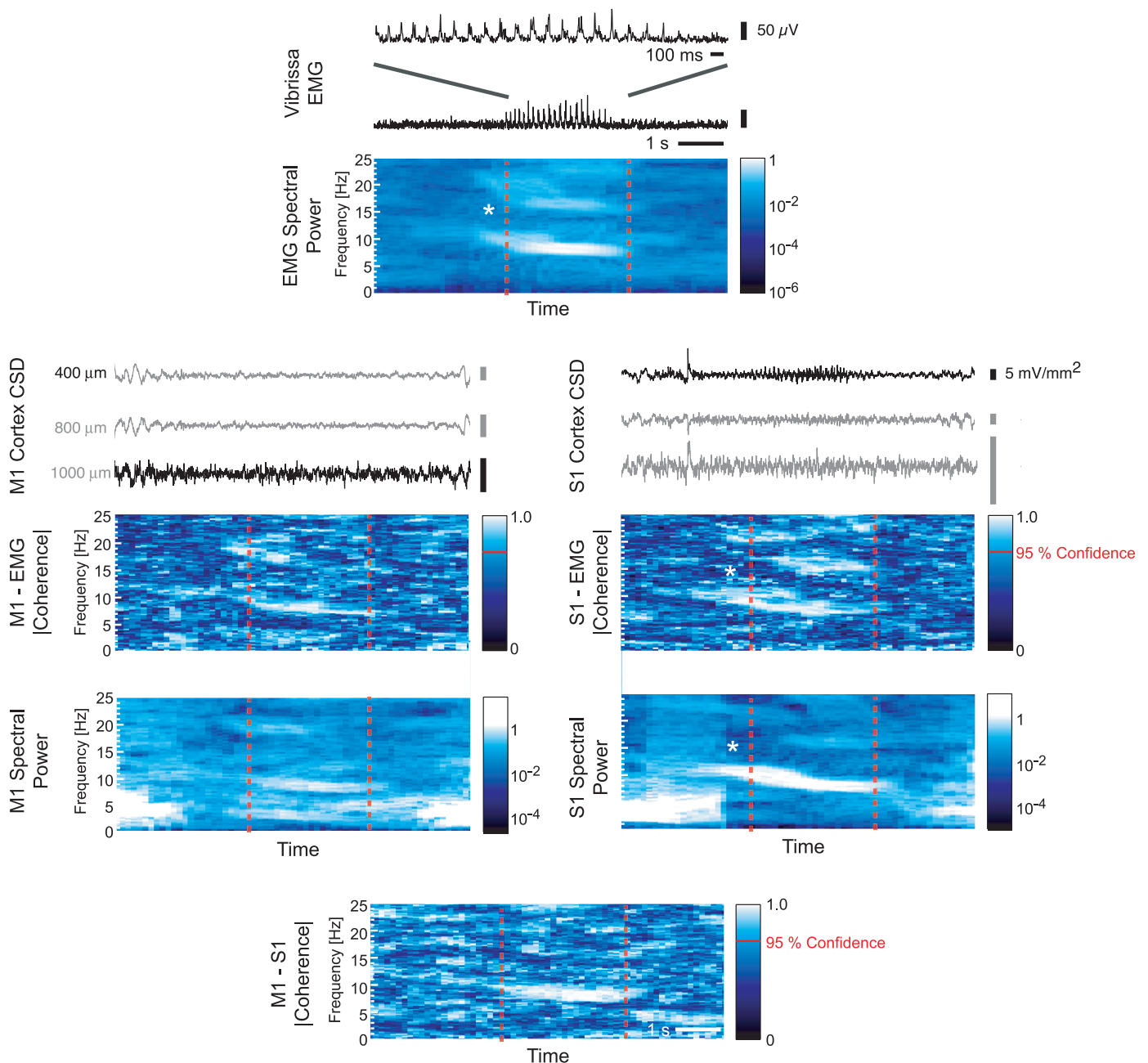


FIG. 3. Example of simultaneously recorded single trial mystacial EMG activity and M1 and S1 cortical activity at 3 depths below the cortical surface. Spectral power of these signals and spectral coherence between these signals are further shown. *Top*: a single epoch of EMG recorded as the animal engaged in rhythmic exploratory whisking. Trace above is an expanded rendering of the whisking epoch, whose nominal temporal boundaries are indicated in all spectra by dashed red lines. The panel below is the spectrogram of the EMG signal, which shows concentration of power at the ~ 8 -Hz fundamental peak; note the logarithmic scale. Spectral power density is derived from 2.0-s windows averaged over 3 tapers to yield a bandwidth (half-width at half-maximum amplitude), or spectral resolution, of $\Delta f = 1.0$ Hz. Analysis window is stepped by 128 ms, $1/8$ of the taper width. *Middle-left*: 1st set of data shows epoch of M1 cortical CSD activity at selected depths. Magnitude of the coherence of the CSD in 1 M1 cortical channel ($1,000 \mu\text{m}$) with the EMG is displayed in the next spectrogram, using the same bandwidth and window parameters as above. White/light blue areas above the red line in the scale bar represent statistically significant ($P < 0.05$) coherence. Spectral power in the same M1 channel is displayed in the 2nd spectrogram; note the saturated scale to highlight the whisking response in the presence of background activity outside of the bout of whisking. *Middle-right*: 1st set of data shows epoch of S1 cortical CSD activity at selected depths. Magnitude of the coherence of the CSD in 1 S1 cortical channel ($400 \mu\text{m}$) with the EMG is displayed in the next spectrogram. Spectral power in the same S1 channel is displayed in the 2nd spectrogram. *Bottom*: magnitude of the coherence between M1 ($1,000\text{-}\mu\text{m}$ channel) and S1 ($400\text{-}\mu\text{m}$ channel) cortices; the channels were selected to give a large signal-to-noise ratio.

ence at the whisking frequency, were obtained for the coherence between the S1 cortical CSD and the EMG (Fig. 4, C and D).

Across all trials and animals ($n = 5$), statistically significant coherence was observed between current flow in M1 cortex and the EMG for superficial as well as deep recordings (Fig.

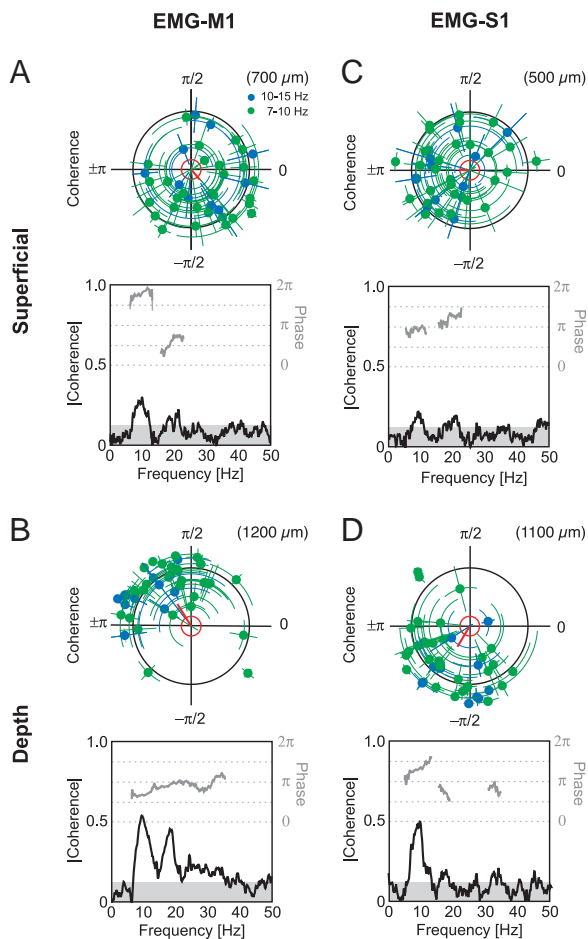


FIG. 4. Coherence between EMG and cortical CSDs at various depths, from 1 animal, over a distribution of trials. *A–D*: *top*: polar plots that show magnitude (radial coordinate) and phase (angular coordinate) of coherence between EMG and cortical CSD at the frequency of maximal EMG power for each 1.5-s epoch. Peak frequency for whisking is binned into 1 of 2 ranges and color-coded. The red radial line is the vector average of coherence across all epochs. Scales: 1) a magnitude of 1.0 is indicated by the length of the 4 radial axes; 2) a black circle marks the 95% confidence level for significant coherence during an individual epochs of whisking, and 3) the inner red circle marks the 95% confidence level for significant coherence of the vector average. Positive phases (clockwise) correspond to a lead of the EMG signal with respect to the CSD signal in the spectral band for whisking. *A–D*: *bottom*: magnitude and phase of the vector averaged spectral coherence as a function of frequency. Shaded regions mark 95% confidence level. Phase spectra are plotted in gray for frequencies where coherence is significant.

2*B*). Similarly significant coherence was observed between current flow in S1 cortex and the EMG (Fig. 2*B*). The coherence between current flow in M1 and S1 cortices was generally quite variable on a trial-to-trial basis. As an average across all trials and animals, the coherence was significant only between currents generated in the superficial layers of M1 and S1 cortex (SS, Fig. 2*C*) and between currents generated in the deep layers (DD, Fig. 2*C*).

Effect of IoN lesion

The observed oscillatory currents in M1 cortex could be derived from sensory input, as was shown to occur for spike signals in sensory cortex (Fee et al. 1997), or from a motor drive that either originates in M1 cortex or provides corollary discharge to M1 cortex. To distinguish among these possibil-

ities, we recorded CSD signals before and after bilateral transection of the IoN. Following transection and with the animal still under anesthesia, there was no evoked electrical activity in response to multi-vibrissa stimulation (cf. Fig. 5, A

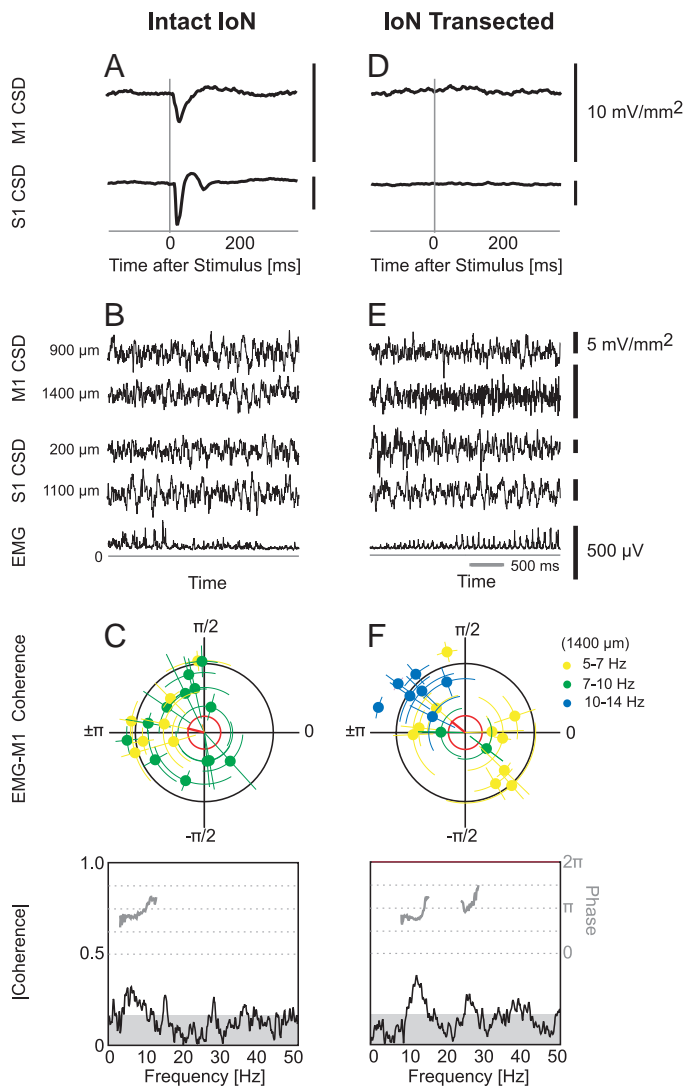


FIG. 5. Evoked responses (in anesthetized state) and whisking-related cortical activity before and after transection of the IoN of the trigeminal nerve. *A* and *D*: average CSD from 100 stimulus repetitions, recorded at a depth of 900 μm in M1 cortex and 200 μm in S1 cortex. Vertical gray lines signify time of stimulation. Time-to-peak (current sink) in motor cortex is greater than that in somatosensory cortex by ~ 3 ms. There was no measurable response after IoN transection. *B* and *E*: *top* 4 traces in each panel are CSD time series recorded at 2 depths each in M1 (900 and 1,400 μm) and S1 cortex (200 and 1,100 μm) during exploratory whisking. Contemporaneous EMG is shown in the 5th trace. *C* and *F*: *top*: polar plots showing coherence between EMG and M1 cortical CSD during whisking behavior, before and after nerve section. Whisking frequencies are color coded in the figure; note increased incidence of 10- to 14-Hz whisking after the lesion. Coherence magnitudes are indicated as in Fig. 2. The black circle marks the 95% confidence level for significant coherence during individual epochs of whisking. The red radial line is the vector average of coherence represented by the dots, and the inner (red) circle marks the 95% confidence level for significance of the average. Positive phases (clockwise) correspond to a lead of CSD signal with respect to EMG signal in the spectral band for whisking. *C* and *F*: *bottom*: magnitude of average coherence spectrum for 1 animal. Shaded regions mark 95% confidence level. Phase spectra are plotted in gray for frequencies where coherence is significant. The shift from low- to high-frequency whisking after sectioning the nerve is evident as a rightward shift of peak coherence.

and *D*). Furthermore, evoked responses were monitored periodically and no animal regained sensitivity in the course of this study, although one animal received a partial transection (~90% lesioned; Fig. 2*A*). Behaviorally, the animals were unresponsive to vibrissa contact and were generally less mobile, but were not unable or unwilling to perform the trained task after transection of the nerve.

We consider the data for one representative animal. Time series of CSD data from M1 cortex, obtained 1 day after the lesion, show remarkably similar modulation by whisking in comparison with data obtained prior to the lesion (cf. Fig. 5, *B* and *E*). The coherence between CSD activity and the EMG here, as before, is highly variable between whisking bouts. Nonetheless, the trial-averaged response is statistically significant after as well as prior to the lesion (cf. Fig. 5, *C* and *F*). In particular, the phase of the coherence before and after the lesion were similar, and the trial-averaged coherence shows strong peaks in the whisking range (cf. Fig. 5, *C* and *F*).

As an average across all trials and animals ($n = 4$), the coherence between the CSD signal in M1 cortex and the EMG remained consistent after transection of the IoN (Fig. 2*B*). The same result was observed for the coherence between the CSD in S1 cortex and the EMG (Fig. 2*B*). Furthermore, there was a marked increase in cortico-cortical coherence involving the superficial motor layers and the deep somatosensory layers (Fig. 2*C*), such that an insignificant prelesion coherence was transformed into a statistically strong coupling after the blockade of sensory input.

DISCUSSION

The flow of electrical current in vibrissa M1 cortex as well as S1 cortex was measured during rhythmic exploratory whisking in the awake rat (Fig. 3). We found that M1 cortex generates intrinsic electrical currents that are phase-locked to the rhythmic, muscular activation of the mystacial pad (Figs. 2–4), which drives the vibrissae. A similar result was found for S1 cortex, in agreement with a past study (O'Connor et al. 2002). Furthermore, phase-locking persisted on bilateral transection of the infraorbital branch of the trigeminal nerve to block all sensory input (Fig. 5). These data show that primary motor cortex either generates a rhythmic output that controls exploratory whisking or receives a copy of the efferent motor output from a different brain area.

Origin of the rhythmic whisking signal in M1 cortex

One interpretation of our results, consistent with the persistence of rhythmic current flow in M1 cortex after transection of the IoN (Figs. 2 and 5) and with the nested, closed loop architecture of the vibrissa sensorimotor pathways (Ahissar and Kleinfeld 2003; Kleinfeld et al. 1999), is that M1 cortex subsumes the role of rhythmic pattern generation during exploratory whisking. This notion is supported by evidence that ablation of M1 cortex disrupts the regular pattern of whisking (Gao et al. 2003). Furthermore, rhythmic microstimulation of vibrissa M1 cortex in awake and aroused animals leads to the two-phase alternation of protraction with retraction seen during exploratory whisking (Berg and Kleinfeld 2003b). Such cycle-by-cycle initiation of whisks would allow the rat to regulate whisking based on sensory feedback, an appealing albeit yet untested scheme for sensorimotor control.

A second interpretation, also consistent with the persistence of rhythmic current flow in M1 cortex after transection of the IoN (Figs. 2 and 5), is that the source of this activity is efference copy. In particular, Welker (1964) showed that rats can produce rhythmic whisking subsequent to varying degrees of cortical ablation. One hypothesis is that structures at the level of the medulla may form a central pattern generator that drives whisking (Gao et al. 2001; Hattox et al. 2003). This suggests that the source of rhythmic current flow in M1 cortex can be efference copy that originates within brain stem structures and ascends to cortex. The existence of such an ascending pathway has not been directly shown, but has also not been ruled out. In the cat, a small fraction of neurons in the facial nucleus also project to the flocculus (Kotchabhakdi and Walberg 1977). Thus, in principle, the cerebellum could act as a conduit for signal flow from the facial motor nucleus, or another medullary nucleus involved in whisking, to ventral lateral thalamus and finally M1 cortex (Jacquin et al. 1989).

Signal flow between S1 and M1

An unexpected observation is that a rhythmic signal persists in S1 cortex after transection of the IoN (Figs. 2*B* and 5*B*). The presence of a motor signal in S1 cortex is certainly consistent with the known topographic connections between vibrissa M1 and S1 cortices (Deschenes et al. 1998; Hoffer et al. 2003; Israeli and Porter 1995; Keller et al. 1996; Kim and Ebner 1999; Veinante and Deschenes 2003). However, it appears inconsistent with the findings of Fee et al. (1997), in which spiking by S1 units in phase with the fast, cycle-by-cycle motion of the vibrissae was largely extinguished on a unilateral lidocaine block of transmission along the contralateral facial nerve. In this experiment, rhythmic whisking on the unblocked, ipsilateral side of the animals served as a control to show that rhythmic activity persisted. The obvious and testable conclusion is that an efferent copy from M1 to S1 cortex is insufficient to drive spiking by the major fraction of neurons in S1 cortex. A second issue is that the current flow in S1 cortex in this work was recorded ≥ 1 days after lesion to the IoN, while the spike signals in the previous work (Fee et al. 1997) were recorded within 1 h of the block. Plasticity could well have affected the efficacy of the M1 to S1 projections on the longer time period (Toldi et al. 1999). Regardless of the solution to this conundrum, it is interesting to speculate that vibrissa S1 cortex has access to both the actual vibrissa position, through afferent input, and the intended position, through an efferent copy from vibrissa M1 cortex (Deschenes et al. 1998). This would allow S1 cortex to compare the two signals as a means to compute perturbations to the intended motion, as can occur when the vibrissae drag along a rough surface (Moore 2004).

ACKNOWLEDGMENTS

We thank D. J. Andersen and J. F. Hetke of the Center for Neural Communication Technology for supplying the multisite probes, M. Deschenes and Q.-T. Nguyen for discussions on anatomy, S. Hefler for assistance with the histology, H. Karten for use of the photomicroscope, G. A. White for assistance with the electronics, and the reviewers for critical comments.

GRANTS

This study was supported by a National Research Science Award fellowship to K. F. Ahrens and National Institute of Mental Health Grant MH-59867 to D. Kleinfeld.

REFERENCES

- Ahissar E and Kleinfeld D.** Closed loop neuronal computations: focus on vibrissa somatosensation in rat. *Cereb Cortex* 13: 53–61, 2003.
- Ahrens KF and Freeman WJ.** Response dynamics of entorhinal cortex in awake, anesthetized, and olfactory bulb-tomized rats. *Brain Res* 911: 193–202, 2001.
- Ahrens KF, Levine H, Suhl H, and Kleinfeld D.** Spectral mixing of rhythmic neuronal signals in sensory cortex. *Proc Natl Acad Sci USA* 99: 15176–15181, 2002.
- Berg RW and Kleinfeld D.** Rhythmic whisking by rat: retraction as well as protraction of the vibrissae is under active muscular control. *J Neurophysiol* 89: 104–117, 2003a.
- Berg RW and Kleinfeld D.** Vibrissa movement elicited by rhythmic electrical microstimulation to motor cortex in the aroused rat mimics exploratory whisking. *J Neurophysiol* 90: 2950–2963, 2003b.
- Brecht M, Preilowski B, and Merzenich MM.** Functional architecture of the mystacial vibrissae. *Behav Brain Res* 84: 81–97, 1997.
- Brecht M, Schneider M, Sakmann B, and Margrie T.** Whisker movements evoked by stimulation of single pyramidal cells in rat motor cortex. *Nature* 427: 704–710, 2004.
- Carvell GE, Miller SA, and Simons DJ.** The relationship of vibrissal motor cortex unit activity to whisking in the awake rat. *Somatosens Motor Res* 13: 115–127, 1996.
- Carvell GE and Simons DJ.** Biometric analyses of vibrissal tactile discrimination in the rat. *J Neurosci* 10: 2638–2648, 1990.
- Carvell GE, Simons DJ, Lichtenstein SH, and Bryant P.** Electromyographic activity of mystacial pad musculature during whisking behavior in the rat. *Somatosens Motor Res* 8: 159–164, 1991.
- Deschenes M, Veinante P, and Zhang Z-W.** The organization of cortico-thalamic pathways: reciprocity versus parity. *Brain Res Brain Res Rev* 28: 286–308, 1998.
- Di S and Barth DS.** Topographic analysis of field potentials in rat vibrissa barrel cortex. *Brain Res* 546: 106–112, 1991.
- Fee MS, Mitra PP, and Kleinfeld D.** Central versus peripheral determines of patterned spike activity in rat vibrissa cortex during whisking. *J Neurophysiol* 78: 1144–1149, 1997.
- Gao P, Bermejo R, and Zeigler HP.** Vibrissa deafferentation and rodent whisking patterns: behavioral evidence for a central pattern generator. *J Neurosci* 21: 5374–5380, 2001.
- Gao P, Hattox AM, Jones LM, Keller A, and Zeigler HP.** Whisker motor cortex ablation and whisker movement patterns. *Somatosens Motor Res* 20: 191–198, 2003.
- Hattox AM, Li Y, and Keller A.** Serotonin regulates rhythmic whisking. *Neuron* 39: 343–352, 2003.
- Hoffer ZS, Hoover JE, and Alloway KD.** Sensorimotor corticocortical projections from rat barrel cortex have an anisotropic organization that facilitates integration of inputs from whiskers in the same row. *J Comp Neurol* 466: 525–544, 2003.
- Hutson KA and Masterton RB.** The sensory contribution of a single vibrissa's cortical barrel. *J Neurophysiol* 56: 1196–1223, 1986.
- Izraeli R and Porter LL.** Vibrissal motor cortex in the rat: connections with the barrel field. *Exp Brain Res* 104: 41–54, 1995.
- Jacquin M, Barcia M, and Rhoades RW.** Structure-function relationships in rat brainstem subnucleus interparietalis: IV. Projection neurons. *J Comp Neurol* 282: 45–62, 1989.
- Jarvis MR and Mitra PP.** Sampling properties of the spectrum and coherency of sequences of action potentials. *Neural Comput* 13: 717–749, 2001.
- Jones MS and Barth DS.** Spatiotemporal organization of fast (>200 Hz) electrical oscillations in rat vibrissa/barrel cortex. *J Neurophysiol* 82: 1599–1609, 1999.
- Kandel A and Buzsaki G.** Cellular-synaptic generation of sleep spindles, spike-and-wave discharges, and evoked thalamocortical responses in the neocortex of the rat. *J Neurosci* 17: 6783–6797, 1997.
- Keller A.** Intrinsic synaptic organization of the motor cortex. *Cereb Cortex* 3: 430–441, 1993.
- Keller A, Weintraub DN, and Miyashita E.** Tactile experience determines the organization of movement representations in rat motor cortex. *Neuroreport* 7: 2373–2378, 1996.
- Kim U and Ebner FF.** Barrels and septa: separate circuits in rat barrels field cortex. *J Comp Neurol* 14: 489–505, 1999.
- Kleinfeld D, Berg RW, and O'Connor SM.** Anatomical loops and their electrical dynamics in relation to whisking by rat. *Somatosens Motor Res* 16: 69–88, 1999.
- Kleinfeld D and Delaney KR.** Distributed representation of vibrissa movement in the upper layers of somatosensory cortex revealed with voltage sensitive dyes. *J Comp Neurol* 375: 89–108, 1996; erratum 378: 594, 1997.
- Kleinfeld D, Sachdev RNS, Merchant LM, Jarvis MR, and Ebner FF.** Adaptive filtering of vibrissa input in motor cortex of rat. *Neuron* 34: 1021–1034, 2002.
- Kotchabhakdi N and Walberg F.** Cerebellar afferents from neurons in motor nuclei of cranial nerves demonstrated by retrograde axonal transport of horseradish peroxidase. *Brain Res* 137: 158–163, 1977.
- Mardia KV, Kent JT, and Bibby JM.** *Multivariate Analysis*. San Diego, CA: Academic Press, 1979.
- Mehta SB and Kleinfeld D.** Frisking the whiskers: patterned sensory input in the rat vibrissa system. *Neuron* 41: 181–184, 2004.
- Mitzdorf U.** Properties of the evoked potential generators: current source-density analysis of visually evoked potentials in the cat cortex. *Neuroscience* 33: 33–59, 1987.
- Moore CI.** Frequency-dependent processing in the vibrissa sensory system. *J Neurophysiol* 91: 2390–2399, 2004.
- Moran DW and Schwartz AB.** Motor cortical activity during drawing movements: population representation during spiral tracing. *J Neurophysiol* 82: 2693–2704, 1999.
- National Institutes of Health.** *Guide for the Care and Use of Laboratory Animals, NIH Publication 85–23*. Bethesda, MD: National Institutes of Health, 1985.
- Nicholson C and Freeman JA.** Theory of current source-density analysis and determination of conductivity tensor for anuran cerebellum. *J Neurophysiol* 38: 356–368, 1975.
- O'Connor SM, Berg RW, and Kleinfeld D.** Coherent electrical activity along vibrissa sensorimotor loops during free whisking in rat. *J Neurophysiol* 87: 2137–2148, 2002.
- Paxinos G and Watson C.** *The Rat Brain in Stereotaxic Coordinates*. San Diego, CA: Academic Press, 1986.
- Prechtl JC, Bullock TH, and Kleinfeld D.** Direct evidence for local oscillatory current sources and intracortical phase gradients in turtle visual cortex. *Proc Natl Acad Sci USA* 97: 877–882, 2000.
- Thomson DJ.** Spectral estimation and harmonic analysis. *Proc IEEE* 70: 1055–1096, 1982.
- Toldi J, Farkas T, Perge J, and Wolff JR.** Facial nerve injury produces a latent somatosensory input through recruitment of the motor cortex in the rat. *Neuroreport* 10: 2143–2147, 1999.
- Veinante P and Deschenes M.** Single-cell study of motor cortex projections to the barrel field in rats. *J Comp Neurol* 464: 98–103, 2003.
- Welker WI.** Analysis of sniffing of the albino rat. *Behaviour* 12: 223–244, 1964.